

Search for Quantum Gravity Using Astrophysical Neutrino Flavour with IceCube

R. Abbasi,¹⁷ M. Ackermann,⁶² J. Adams,¹⁸ J. A. Aguilar,¹² M. Ahlers,²² M. Ahrens,⁵³ J.M. Alameddine,²³ C. Alispach,²⁸ A. A. Alves Jr.,³¹ N. M. Amin,⁴⁵ K. Andeen,⁴³ T. Anderson,⁵⁹ G. Anton,²⁶ C. Argüelles,¹⁴ Y. Ashida,⁴¹ S. Axani,¹⁵ X. Bai,⁴⁹ A. Balagopal V.,⁴¹ A. Barbano,²⁸ S. W. Barwick,³⁰ B. Bastian,⁶² V. Basu,⁴¹ S. Baur,¹² R. Bay,⁸ J. J. Beatty,^{20,21} K.-H. Becker,⁶¹ J. Becker Tjus,¹¹ C. Bellenghi,²⁷ S. BenZvi,⁵¹ D. Berley,¹⁹ E. Bernardini,⁶² * D. Z. Besson,³⁴ † G. Binder,^{8,9} D. Bindig,⁶¹ E. Blaufuss,¹⁹ S. Blot,⁶² M. Boddenberg,¹ F. Bontempo,³¹ J. Borowka,¹ S. Böser,⁴² O. Botner,⁶⁰ J. Böttcher,¹ E. Bourbeau,²² F. Bradascio,⁶² J. Braun,⁴¹ B. Brinson,⁶ S. Bron,²⁸ J. Brostean-Kaiser,⁶² S. Browne,³² A. Burgman,⁶⁰ R. T. Burley,² R. S. Busse,⁴⁴ M. A. Campana,⁴⁸ E. G. Carnie-Bronca,² C. Chen,⁶ Z. Chen,⁵⁴ D. Chirkin,⁴¹ K. Choi,⁵⁵ B. A. Clark,²⁴ K. Clark,³³ L. Classen,⁴⁴ A. Coleman,⁴⁵ G. H. Collin,¹⁵ J. M. Conrad,¹⁵ P. Coppin,¹³ P. Correa,¹³ D. F. Cowen,^{58,59} R. Cross,⁵¹ C. Dappen,¹ P. Dave,⁶ C. De Clercq,¹³ J. J. DeLaunay,⁵⁷ D. Delgado López,¹⁴ H. Dembinski,⁴⁵ K. Deoskar,⁵³ A. Desai,⁴¹ P. Desiati,⁴¹ K. D. de Vries,¹³ G. de Wasseige,³⁸ M. de With,¹⁰ T. DeYoung,²⁴ A. Diaz,¹⁵ J. C. Díaz-Vélez,⁴¹ M. Dittmer,⁴⁴ H. Dujmovic,³¹ M. Dunkman,⁵⁹ M. A. DuVernois,⁴¹ E. Dvorak,⁴⁹ T. Ehrhardt,⁴² P. Eller,²⁷ R. Engel,^{31,32} H. Erpenbeck,¹ J. Evans,¹⁹ P. A. Evenson,⁴⁵ K. L. Fan,¹⁹ K. Farrag,³⁶ A. R. Fazely,⁷ N. Feigl,¹⁰ S. Fiedlschuster,²⁶ A. T. Fienberg,⁵⁹ K. Filimonov,⁸ C. Finley,⁵³ L. Fischer,⁶² D. Fox,⁵⁸ A. Franckowiak,^{11,62} E. Friedman,¹⁹ A. Fritz,⁴² P. Fürst,¹ T. K. Gaisser,⁴⁵ J. Gallagher,⁴⁰ E. Ganster,¹ A. Garcia,¹⁴ S. Garrappa,⁶² L. Gerhardt,⁹ A. Ghadimi,⁵⁷ C. Glaser,⁶⁰ T. Glauch,²⁷ T. Glüsenskamp,²⁶ J. G. Gonzalez,⁴⁵ S. Goswami,⁵⁷ D. Grant,²⁴ T. Grégoire,⁵⁹ S. Griswold,⁵¹ C. Günther,¹ P. Gutjahr,²³ C. Haack,²⁷ A. Hallgren,⁶⁰ R. Halliday,²⁴ L. Halve,¹ F. Halzen,⁴¹ M. Ha Minh,²⁷ K. Hanson,⁴¹ J. Hardin,⁴¹ A. A. Harnisch,²⁴ A. Haungs,³¹ D. Hebecker,¹⁰ K. Helbing,⁶¹ F. Henningsen,²⁷ E. C. Hettinger,²⁴ S. Hickford,⁶¹ J. Hignight,²⁵ C. Hill,¹⁶ G. C. Hill,² K. D. Hoffman,¹⁹ R. Hoffmann,⁶¹ B. Hokanson-Fasig,⁴¹ K. Hoshina,⁴¹ ‡ F. Huang,⁵⁹ M. Huber,²⁷ T. Huber,³¹ K. Hultqvist,⁵³ M. Hünnefeld,²³ R. Hussain,⁴¹ K. Hymon,²³ S. In,⁵⁵ N. Iovine,¹² A. Ishihara,¹⁶ M. Jansson,⁵³ G. S. Japaridze,⁵ M. Jeong,⁵⁵ M. Jin,¹⁴ B. J. P. Jones,⁴ D. Kang,³¹ W. Kang,⁵⁵ X. Kang,⁴⁸ A. Kappes,⁴⁴ D. Kappesser,⁴² L. Kardum,²³ T. Karg,⁶² M. Karl,²⁷ A. Karle,⁴¹ T. Katori,³⁵ U. Katz,²⁶ M. Kauer,⁴¹ M. Kellermann,¹ J. L. Kelley,⁴¹ A. Kheirandish,⁵⁹ K. Kin,¹⁶ T. Kintscher,⁶² J. Kiryluk,⁵⁴ S. R. Klein,^{8,9} R. Koirala,⁴⁵ H. Kolanoski,¹⁰ T. Kontrimas,²⁷ L. Köpke,⁴² C. Kopper,²⁴ S. Kopper,⁵⁷ D. J. Koskinen,²² P. Koundal,³¹ M. Kovacevich,⁴⁸ M. Kowalski,^{10,62} T. Kozynets,²² E. Kun,¹¹ N. Kurahashi,⁴⁸ N. Lad,⁶² C. Lagunas Gualda,⁶² J. L. Lanfranchi,⁵⁹ M. J. Larson,¹⁹ F. Lauber,⁶¹ J. P. Lazar,^{14,41} J. W. Lee,⁵⁵ K. Leonard,⁴¹ A. Leszczyńska,³² Y. Li,⁵⁹ M. Lincetto,¹¹ Q. R. Liu,⁴¹ M. Liubarska,²⁵ E. Lohfink,⁴² C. J. Lozano Mariscal,⁴⁴ L. Lu,⁴¹ F. Lucarelli,²⁸ A. Ludwig,^{24,37} W. Luszczak,⁴¹ Y. Lyu,^{8,9} W. Y. Ma,⁶² J. Madsen,⁴¹ K. B. M. Mahn,²⁴ Y. Makino,⁴¹ S. Mancina,⁴¹ S. Mandalia,³⁶ I. C. Mariş,¹² I. Martinez-Soler,¹⁴ R. Maruyama,⁴⁶ K. Mase,¹⁶ T. McElroy,²⁵ F. McNally,³⁹ J. V. Mead,²² K. Meagher,⁴¹ S. Mechbal,⁶² A. Medina,²¹ M. Meier,¹⁶ S. Meighen-Berger,²⁷ J. Micallef,²⁴ D. Mockler,¹² T. Montaruli,²⁸ R. W. Moore,²⁵ R. Morse,⁴¹ M. Moulai,¹⁵ R. Naab,⁶² R. Nagai,¹⁶ U. Naumann,⁶¹ J. Necker,⁶² L. V. Nguyen,²⁴ H. Niederhausen,²⁷ M. U. Nisa,²⁴ S. C. Nowicki,²⁴ A. Obertacke Pollmann,⁶¹ M. Oehler,³¹ B. Oeyen,²⁹ A. Olivas,¹⁹ E. O'Sullivan,⁶⁰ H. Pandya,⁴⁵ D. V. Pankova,⁵⁹ N. Park,³³ G. K. Parker,⁴ E. N. Paudel,⁴⁵ L. Paul,⁴³ C. Pérez de los Heros,⁶⁰ L. Peters,¹ J. Peterson,⁴¹ S. Philippen,¹ S. Pieper,⁶¹ M. Pittermann,³² A. Pizzuto,⁴¹ M. Plum,⁴³ Y. Popovych,⁴² A. Porcelli,²⁹ M. Prado Rodriguez,⁴¹ P. B. Price,⁸ B. Pries,²⁴ G. T. Przybylski,⁹ C. Raab,¹² A. Raissi,¹⁸ M. Rameez,²² K. Rawlins,³ I. C. Rea,²⁷ A. Rehman,⁴⁵ P. Reichherzer,¹¹ R. Reimann,¹ G. Renzi,¹² E. Resconi,²⁷ S. Reusch,⁶² W. Rhode,²³ M. Richman,⁴⁸ B. Riedel,⁴¹ E. J. Roberts,² S. Robertson,^{8,9} G. Roellinghoff,⁵⁵ M. Rongen,⁴² C. Rott,^{52,55} T. Ruhe,²³ D. Ryckbosch,²⁹ D. Rysewyk Cantu,²⁴ I. Safa,^{14,41} J. Saffer,³² S. E. Sanchez Herrera,²⁴ A. Sandrock,²³ J. Sandroos,⁴² M. Santander,⁵⁷ S. Sarkar,⁴⁷ S. Sarkar,²⁵ K. Satalecka,⁶² M. Schaufel,¹ H. Schieler,³¹ S. Schindler,²⁶ T. Schmidt,¹⁹ A. Schneider,⁴¹ J. Schneider,²⁶ F. G. Schröder,^{31,45} L. Schumacher,²⁷ G. Schwefer,¹ S. Sclafani,⁴⁸ D. Seckel,⁴⁵ S. Seunarine,⁵⁰ A. Sharma,⁶⁰ S. Shefali,³² M. Silva,⁴¹ B. Skrzypek,¹⁴ B. Smithers,⁴ R. Snihur,⁴¹ J. Soedingrekso,²³ D. Soldin,⁴⁵ C. Spannfellner,²⁷ G. M. Spiczak,⁵⁰ C. Spiering,⁶² † J. Stachurska,⁶² M. Stamatikos,²¹ T. Stanev,⁴⁵ R. Stein,⁶² J. Stettner,¹ A. Steuer,⁴² T. Stezelberger,⁹ T. Stürwald,⁶¹ T. Stuttard,²² G. W. Sullivan,¹⁹ I. Taboada,⁶ S. Ter-Antonyan,⁷ S. Tilav,⁴⁵ F. Tischbein,¹ K. Tollefson,²⁴ C. Tönnis,⁵⁶ S. Toscano,¹² D. Tosi,⁴¹ A. Trettin,⁶² M. Tselengidou,²⁶ C. F. Tung,⁶ A. Turcati,²⁷ R. Turcotte,³¹ C. F. Turley,⁵⁹ J. P. Twagirayezu,²⁴ B. Ty,⁴¹ M. A. Unland Elorrieta,⁴⁴ N. Valtonen-Mattila,⁶⁰ J. Vandenbroucke,⁴¹ N. van Eijndhoven,¹³ D. Vannerom,¹⁵ J. van Santen,⁶² S. Verpoest,²⁹ C. Walck,⁵³ T. B. Watson,⁴ C. Weaver,²⁴ P. Weigel,¹⁵ A. Weindl,³¹ M. J. Weiss,⁵⁹ J. Weldert,⁴² C. Wendt,⁴¹ J. Werthebach,²³ M. Weyrauch,³² N. Whitehorn,^{24,37} C. H. Wiebusch,¹ D. R. Williams,⁵⁷ M. Wolf,²⁷ K. Woschnagg,⁸ G. Wrede,²⁶ J. Wulff,¹¹ X. W. Xu,⁷ J. P. Yanez,²⁵ S. Yoshida,¹⁶ S. Yu,²⁴ T. Yuan,⁴¹ Z. Zhang,⁵⁴ and P. Zhelnin¹⁴

(IceCube Collaboration)

¹*III. Physikalisches Institut, RWTH Aachen University, D-52056 Aachen, Germany*

²*Department of Physics, University of Adelaide, Adelaide, 5005, Australia*

³*Dept. of Physics and Astronomy, University of Alaska Anchorage, 3211 Providence Dr., Anchorage, AK 99508, USA*

⁴*Dept. of Physics, University of Texas at Arlington, 502 Yates St.,*

- Science Hall Rm 108, Box 19059, Arlington, TX 76019, USA
- ⁵CTSPS, Clark-Atlanta University, Atlanta, GA 30314, USA
- ⁶School of Physics and Center for Relativistic Astrophysics, Georgia Institute of Technology, Atlanta, GA 30332, USA
- ⁷Dept. of Physics, Southern University, Baton Rouge, LA 70813, USA
- ⁸Dept. of Physics, University of California, Berkeley, CA 94720, USA
- ⁹Lawrence Berkeley National Laboratory, Berkeley, CA 94720, USA
- ¹⁰Institut für Physik, Humboldt-Universität zu Berlin, D-12489 Berlin, Germany
- ¹¹Fakultät für Physik & Astronomie, Ruhr-Universität Bochum, D-44780 Bochum, Germany
- ¹²Université Libre de Bruxelles, Science Faculty CP230, B-1050 Brussels, Belgium
- ¹³Vrije Universiteit Brussel (VUB), Dienst ELEM, B-1050 Brussels, Belgium
- ¹⁴Department of Physics and Laboratory for Particle Physics and Cosmology, Harvard University, Cambridge, MA 02138, USA
- ¹⁵Dept. of Physics, Massachusetts Institute of Technology, Cambridge, MA 02139, USA
- ¹⁶Dept. of Physics and Institute for Global Prominent Research, Chiba University, Chiba 263-8522, Japan
- ¹⁷Department of Physics, Loyola University Chicago, Chicago, IL 60660, USA
- ¹⁸Dept. of Physics and Astronomy, University of Canterbury, Private Bag 4800, Christchurch, New Zealand
- ¹⁹Dept. of Physics, University of Maryland, College Park, MD 20742, USA
- ²⁰Dept. of Astronomy, Ohio State University, Columbus, OH 43210, USA
- ²¹Dept. of Physics and Center for Cosmology and Astro-Particle Physics, Ohio State University, Columbus, OH 43210, USA
- ²²Niels Bohr Institute, University of Copenhagen, DK-2100 Copenhagen, Denmark
- ²³Dept. of Physics, TU Dortmund University, D-44221 Dortmund, Germany
- ²⁴Dept. of Physics and Astronomy, Michigan State University, East Lansing, MI 48824, USA
- ²⁵Dept. of Physics, University of Alberta, Edmonton, Alberta, Canada T6G 2E1
- ²⁶Erlangen Centre for Astroparticle Physics, Friedrich-Alexander-Universität Erlangen-Nürnberg, D-91058 Erlangen, Germany
- ²⁷Physik-department, Technische Universität München, D-85748 Garching, Germany
- ²⁸Département de physique nucléaire et corpusculaire, Université de Genève, CH-1211 Genève, Switzerland
- ²⁹Dept. of Physics and Astronomy, University of Gent, B-9000 Gent, Belgium
- ³⁰Dept. of Physics and Astronomy, University of California, Irvine, CA 92697, USA
- ³¹Karlsruhe Institute of Technology, Institute for Astroparticle Physics, D-76021 Karlsruhe, Germany
- ³²Karlsruhe Institute of Technology, Institute of Experimental Particle Physics, D-76021 Karlsruhe, Germany
- ³³Dept. of Physics, Engineering Physics, and Astronomy, Queen's University, Kingston, ON K7L 3N6, Canada
- ³⁴Dept. of Physics and Astronomy, University of Kansas, Lawrence, KS 66045, USA
- ³⁵Dept. of Physics, King's College London, London WC2R 2LS, UK
- ³⁶Dept. of Physics and Astronomy, Queen Mary University of London, London E1 4NS, UK
- ³⁷Department of Physics and Astronomy, UCLA, Los Angeles, CA 90095, USA
- ³⁸Centre for Cosmology, Particle Physics and Phenomenology - CP3, Université catholique de Louvain, Louvain-la-Neuve, Belgium
- ³⁹Department of Physics, Mercer University, Macon, GA 31207-0001, USA
- ⁴⁰Dept. of Astronomy, University of Wisconsin–Madison, Madison, WI 53706, USA
- ⁴¹Dept. of Physics and Wisconsin IceCube Particle Astrophysics Center, University of Wisconsin–Madison, Madison, WI 53706, USA
- ⁴²Institute of Physics, University of Mainz, Staudinger Weg 7, D-55099 Mainz, Germany
- ⁴³Department of Physics, Marquette University, Milwaukee, WI, 53201, USA
- ⁴⁴Institut für Kernphysik, Westfälische Wilhelms-Universität Münster, D-48149 Münster, Germany
- ⁴⁵Bartol Research Institute and Dept. of Physics and Astronomy, University of Delaware, Newark, DE 19716, USA
- ⁴⁶Dept. of Physics, Yale University, New Haven, CT 06520, USA
- ⁴⁷Dept. of Physics, University of Oxford, Parks Road, Oxford OX1 3PU, UK
- ⁴⁸Dept. of Physics, Drexel University, 3141 Chestnut Street, Philadelphia, PA 19104, USA
- ⁴⁹Physics Department, South Dakota School of Mines and Technology, Rapid City, SD 57701, USA
- ⁵⁰Dept. of Physics, University of Wisconsin, River Falls, WI 54022, USA
- ⁵¹Dept. of Physics and Astronomy, University of Rochester, Rochester, NY 14627, USA
- ⁵²Department of Physics and Astronomy, University of Utah, Salt Lake City, UT 84112, USA
- ⁵³Oskar Klein Centre and Dept. of Physics, Stockholm University, SE-10691 Stockholm, Sweden
- ⁵⁴Dept. of Physics and Astronomy, Stony Brook University, Stony Brook, NY 11794-3800, USA
- ⁵⁵Dept. of Physics, Sungkyunkwan University, Suwon 16419, Korea
- ⁵⁶Institute of Basic Science, Sungkyunkwan University, Suwon 16419, Korea
- ⁵⁷Dept. of Physics and Astronomy, University of Alabama, Tuscaloosa, AL 35487, USA
- ⁵⁸Dept. of Astronomy and Astrophysics, Pennsylvania State University, University Park, PA 16802, USA
- ⁵⁹Dept. of Physics, Pennsylvania State University, University Park, PA 16802, USA
- ⁶⁰Dept. of Physics and Astronomy, Uppsala University, Box 516, S-75120 Uppsala, Sweden
- ⁶¹Dept. of Physics, University of Wuppertal, D-42119 Wuppertal, Germany
- ⁶²DESY, D-15738 Zeuthen, Germany

Along their long propagation from production to detection, neutrino states undergo quantum interference which converts their types, or flavours [1, 2]. High-energy astrophysical neutrinos, first observed by the IceCube Neutrino Observatory [3], are known to propagate unperturbed over a billion light years in vacuum [4]. These neutrinos act as the largest quantum interferometer and are sensitive to the smallest effects in vacuum due to new physics. Quantum gravity (QG) [5] aims to describe gravity in a quantum mechanical framework, unifying matter, forces and space-time. QG effects are expected to appear at the ultra-high-energy scale known as the Planck energy, $E_p \equiv 1.22 \times 10^{19}$ giga-electronvolts (GeV). Such a high-energy universe would have existed only right after the Big Bang and it is inaccessible by human technologies. On the other hand, it is speculated that the effects of QG may exist in our low-energy vacuum [6–8], but are suppressed by the Planck energy as E_p^{-1} ($\sim 10^{-19}$ GeV $^{-1}$), E_p^{-2} ($\sim 10^{-38}$ GeV $^{-2}$), or its higher powers. The coupling of particles to these effects are too small to measure in kinematic observables, but the phase shift of neutrino waves could cause observable flavour conversions. Here, we report the first result of neutrino interferometry [9] using astrophysical neutrino flavours [10, 11] to search for new space-time structure. We did not find any evidence of anomalous flavour conversion in IceCube astrophysical neutrino flavour data. We place the most stringent limits of any known technologies, down to 10^{-42} GeV $^{-2}$, on the dimension-six operators that parameterize the space-time defects for preferred astrophysical production scenarios. For the first time, we unambiguously reach the signal region of quantum-gravity-motivated physics.

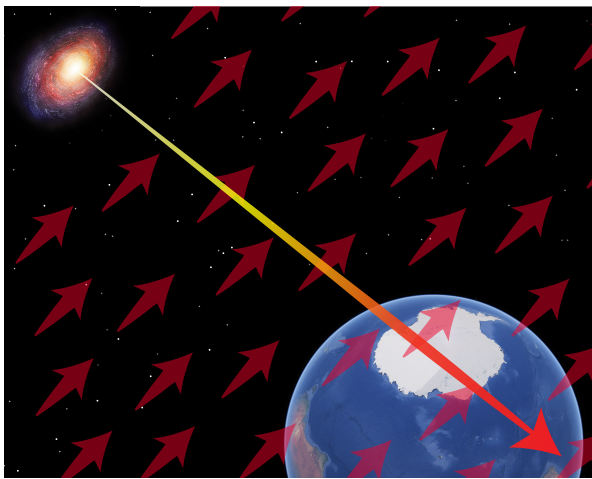


FIG. 1. *Illustration of this analysis.* High-energy astrophysical neutrinos, from 60 TeV to 2 PeV, are emitted from distant high-energy sources (shown by a long arrow). The neutrino propagation may be affected by space-time defects which can be viewed as an aether-like media in vacuum, and in general these defects have directions depicted by red arrows. Although the effect may depend on directions, we assume it is isotropic in our frame without loss of generality as data is compatible with an isotropic distribution [10].

In the past, QG was searched for through astrophysical neutrino spectrum distortion [12] and time-of-flight [13] measurements. Here, we focus on astrophysical neutrino flavour information to search for QG effects via neutrino interferometry. Neutrino interferometry [9] has been applied in various terrestrial neutrino experiments; however no evidence of QG has been found [14]. The sensitivity of neutrino interferometry for astrophysical neutrinos exceeds any terrestrial experiments because of the higher energies and longer propagation distances of the neutrinos involved; see Fig. 1 for an illustration.

Neutrino interactions with low-energy manifestations of

QG can be modelled using effective operators [9], such as

$$H \sim \frac{m^2}{2E} + \hat{a}^{(3)} - E \cdot \hat{c}^{(4)} + E^2 \cdot \hat{a}^{(5)} - E^3 \cdot \hat{c}^{(6)} \dots \quad (1)$$

The first term in this Hamiltonian describes the neutrino mass term [15], where we assume the normal mass ordering. All other terms include new physics operators ($\hat{a}^{(3)}$, $\hat{c}^{(4)}$, $\hat{a}^{(5)}$, $\hat{c}^{(6)}$, ...) are new physics operators representing new interactions such as those between neutrinos and space-time defects. These terms correspond to the isotropic part of the Standard-Model Extension (SME) [16], which is an effective field theory that describes the effects of particle Lorentz violation. All terms are 3×3 complex matrices in the neutrino flavour basis. There are three neutrino flavours: electron-neutrino (ν_e), muon-neutrino (ν_μ), and tau-neutrino (ν_τ). The solution of this Hamiltonian describes the evolution of neutrino flavours. Because astrophysical flux normalisation is unknown, neutrino flavour is measured in terms of the flavour ratio ($\nu_e : \nu_\mu : \nu_\tau$), which is a normalized fraction of each flavour defined after integrating expected astrophysical neutrino spectra. The measured flavour ratio depends on the production mechanisms of astrophysical neutrinos at their sources and on the effective Hamiltonian. Appendix A contains further details of our formulation.

The IceCube Neutrino Observatory [17] is an array of 5,160 digital optical modules (DOMs) embedded in the Antarctic ice between 1,450 m to 2,450 m below the surface. Each DOM contains one 25.4 cm photo-multiplier tube in a glass shell, and it detects light from charged particles produced by neutrino interactions. A series of 60 DOMs are connected with a vertical spacing of 17 m to make one string, and 86 strings with ~ 125 m separation cover 1 km 3 volume of natural ice as a target volume for astrophysical neutrinos.

When neutrinos undergo charged-current (CC) interactions, they generate charged leptons whose types depend on the neutrino flavours. Namely, an ν_e ($\bar{\nu}_e$) creates an electron (positron), a ν_μ ($\bar{\nu}_\mu$) creates a muon (anti-muon), and a ν_τ ($\bar{\nu}_\tau$) creates a tau (anti-tau). These charged leptons generate characteristic light emission distributions in IceCube. Electrons

initiate electromagnetic showers in ice that look like an approximately isotropic emission of photons (cascade); muons emit light along their straight trajectories (track); and some taus produce an isotropic emission with a slight elongation, reflecting bursts of photon emission from the production of the tau and its subsequent decay (double cascade). However, most taus from CC interactions and hadronic showers from neutral-current (NC) interactions also lead to cascades. A likelihood function is constructed from the time and charge distributions of DOMs to estimate the energies, directions, and flavours of neutrinos. Charged leptons and charged anti-leptons have indistinguishable light emission profiles in ice.

In this analysis, we use the high-energy starting event (HESE) sample with 7.5 years of data collection during 2010 to 2018 [10]. A total of 60 events are observed above 60 TeV. Among them, 41, 17, and two events are classified as cascades, tracks, and double cascades, respectively. Cascades and tracks are distributed in 10 incoming zenith angle bins, in the range $\cos \theta_z = [-1.0, +1.0]$, with $\cos \theta_z = +1.0$ pointing to the celestial south pole. We use 20 natural logarithmic bins in deposited energy in the range $E = [60 \text{ TeV}, 2 \text{ PeV}]$. For the double cascade events, there are 10 bins in the reconstructed distance between two cascade signals $L = [10 \text{ m}, 100 \text{ m}]$ instead of zenith angle bins.

The expected number of events in each bin is computed through a Monte Carlo (MC) simulation. First, the astrophysical neutrino flux is modeled as a single power-law spectrum. This is weighted with the assumed flavour ratio at the source and the mixing probability derived from the effective Hamiltonian including new physics operators (Eq. 1). The foreground flux due to atmospheric neutrinos from π and K -decays [18], charm meson decays [19], and atmospheric muons [20], is added to simulate the complete flux arriving at the detector. Neutrino absorption in the Earth is modeled using a standard Earth density profile [21]. Particles produced by neutrino interactions [22] are computed using specialised MC [23] to output photon signals.

Fig. 2 shows a comparison of the HESE 7.5-yr flavour ratio measurement [11] with model predictions. This flavour triangle diagram represents astrophysical neutrino flavour ratios where one point in this diagram shows the energy-averaged flavour composition at Earth. The pink region near the centre denotes the so-called standard scenarios. This represents all possible flavour ratios at Earth from standard astrophysical neutrino production mechanisms via neutrino mixing [24]. As shown, all of the standard flavour ratios are enclosed in the 95% confidence level (C.L.) contour, which implies that, at this moment, all models within standard scenarios are allowed. In other words, the IceCube HESE flavour measurement is consistent with the standard scenarios, given current statistics and systematic errors. However, current data excludes certain QG models that produce flavour compositions far away from the standard region because any new structure in the vacuum would produce detectable anomalous flavour ratios, shown by lines in Fig. 2.

In order to make quantitative statement on these scenarios,

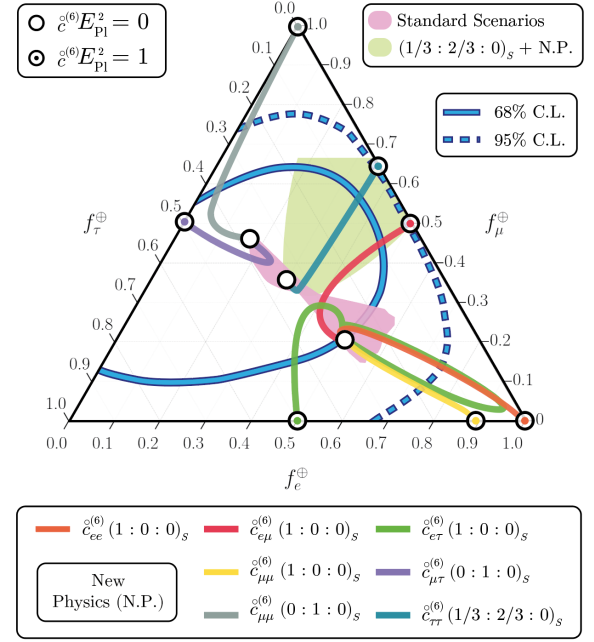


FIG. 2. *Astrophysical neutrino flavour triangle, including illustrations of new physics effects and data contours.* The figure represents the flavour ratio ($\nu_e : \nu_\mu : \nu_\tau$) of given compositions at the source (S), where the corners indicate pure ν_e , ν_μ , or ν_τ composition. The blue solid and dashed lines show 68% and 95% C.L. contours [11] from IceCube data. The pink region represents expected flavour ratios from the standard astrophysical neutrino production models, where the neutrinos at the production source are all possible combinations of ν_e and ν_μ with the neutrino oscillation parameter errors given in [15]. The lines explained in the lower legend illustrate the effects of the $\hat{c}^{(6)}$ new physics (NP) operators. Three astrophysical neutrino production models are highlighted by \bigcirc symbols, a ν_μ dominant source ($0 : 1 : 0$) $_S$ (top), a ν_e dominant source ($1 : 0 : 0$) $_S$ (bottom), and a preferred model ($1/3 : 2/3 : 0$) $_S$ (middle). When NP operators are small ($\leq m^2/2E$), they are distributed within the central region. If the values of NP operators are increased, predicted flavour ratios start to move away from the centre, and they reach to \odot symbols with the large NP such as $\hat{c}^{(6)} = E_p^{-2}$. For simplicity we concentrate on real, positive new physics potentials.

we perform a likelihood analysis and report results using a Bayesian method. Our analysis includes all of the flux components previously discussed in the text and implements their systematics according to the prescription given in [10]. Our analysis likelihood includes: nuisance parameters to incorporate the flux and detector uncertainties, standard oscillation parameters and neutrino mass differences, and parameters that incorporate the QG effective operators. Appendix B includes technical details of the fit methods and on the systematic errors.

Figure 3 shows results for the dimension-six operators. Results of other operators are summarized in Appendix C. These represent new physics interactions and we expect the QG-motivated physics operator to be of order $E_p^{-2} = 6.7 \times 10^{-39} \text{ GeV}^{-2}$. Limits are shown on a log-scale. The right

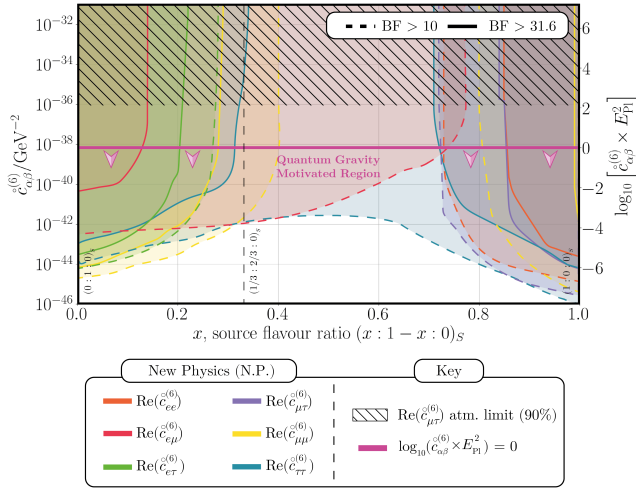


FIG. 3. **Limits on the dimension-six new physics operator.** The QG-motivated physics signal region is defined by $\log_{10}(c_{ij}^{(6)} \cdot E_p^2) < 0$. The hatched region is the limit obtained from the atmospheric neutrino data analysis on $\text{Re}(c_{\mu\tau}^{(6)})$ [9]. Limits are presented as a function of the assumed astrophysical neutrino flavour ratio at the production source. The leftmost scenario is ν_μ dominant $(0:1:0)_S$ and the rightmost is ν_e dominant $(1:0:0)_S$. The preferred scenario corresponds to $(1/3:2/3:0)_S$ (dashed vertical line). Limits on $\text{Re}(c_{ee}^{(6)})$ (orange), $\text{Re}(c_{e\mu}^{(6)})$ (red), $\text{Re}(c_{e\tau}^{(6)})$ (green), $\text{Re}(c_{\mu\mu}^{(6)})$ (yellow), $\text{Re}(c_{\mu\tau}^{(6)})$ (purple), and $\text{Re}(c_{\tau\tau}^{(6)})$ (blue) are shown.

axis incorporates an additional E_p^2 factor where below zero corresponds to the QG-motivated physics signal region. For the first time, we reach the QG-motivated signal region of the dimension-six operator with neutrinos. The limits are a function of the astrophysical neutrino production model at the source. Strong limits are obtained for ν_μ dominant $(0:1:0)_S$ and ν_e dominant $(1:0:0)_S$ scenarios. Weaker limits for the preferred scenario $(1/3:2/3:0)_S$ are also obtained. This can be inferred from Fig. 2 because $(1/3:2/3:0)_S$ with new physics scenarios described by the green region, is almost covered by the 95% C.L. contour.

In Table I, limits obtained from Bayes factor > 31.6 are quoted for three source flavour ratio scenarios. Although the motivation of this analysis is to look for evidence of QG, the formalism we have used is model-independent, and our results can set limits on various new physics models [25]. For example, the limits for dimension three operators shown in the first group of Table I can be interpreted as a limit on a new long-range force [26], neutrino-dark energy coupling [27], neutrino-dark matter scattering [28], *etc.*

In summary, we have performed the seminal work using astrophysical neutrino flavour information to search for the footprint of QG. We have not found any evidence of QG, but for the first time, we have reached QG-motivated parameter space for dimension six operators. In doing so, we have placed the strongest limits on effective operators that parameterize QG effects across all fields of science.

The IceCube collaboration acknowledges the significant

dim	coefficient	limit	dim	coefficient	limit	$(\phi_e^i : \phi_\mu^i : \phi_\tau^i)_S$
3	$\text{Re}(a_{\mu\mu}^{(5)})$	$6 \times 10^{-26} \text{ GeV}$	4	$\text{Re}(c_{e\mu}^{(6)})$	2×10^{-31}	$(0:1:0)_S$
	$\text{Re}(a_{e\tau}^{(5)})$	$3 \times 10^{-27} \text{ GeV}$		$\text{Re}(c_{e\tau}^{(6)})$	7×10^{-33}	$(0:1:0)_S$
	$\text{Re}(a_{\mu\tau}^{(5)})$	$3 \times 10^{-27} \text{ GeV}$		$\text{Re}(c_{\mu\mu}^{(6)})$	4×10^{-33}	$(0:1:0)_S$
	$\text{Re}(a_{\tau\tau}^{(5)})$	$5 \times 10^{-27} \text{ GeV}$		$\text{Re}(c_{\tau\tau}^{(6)})$	1×10^{-32}	$(0:1:0)_S$
	$\text{Re}(a_{ee}^{(3)})$	$4 \times 10^{-28} \text{ GeV}$		$\text{Re}(c_{ee}^{(4)})$	6×10^{-33}	$(1:0:0)_S$
	$\text{Re}(a_{e\mu}^{(3)})$	$6 \times 10^{-27} \text{ GeV}$		$\text{Re}(c_{e\mu}^{(4)})$	7×10^{-34}	$(1:0:0)_S$
	$\text{Re}(a_{e\tau}^{(3)})$	$2 \times 10^{-27} \text{ GeV}$	$\text{Re}(c_{e\tau}^{(4)})$	8×10^{-34}	$(1:0:0)_S$	
5	$\text{Re}(a_{e\mu}^{(5)})$	$3 \times 10^{-36} \text{ GeV}^{-1}$	6	$\text{Re}(c_{e\mu}^{(6)})$	$4 \times 10^{-41} \text{ GeV}^{-2}$	$(0:1:0)_S$
	$\text{Re}(a_{e\tau}^{(5)})$	$9 \times 10^{-39} \text{ GeV}^{-1}$		$\text{Re}(c_{e\tau}^{(6)})$	$3 \times 10^{-44} \text{ GeV}^{-2}$	$(0:1:0)_S$
	$\text{Re}(a_{\mu\mu}^{(5)})$	$8 \times 10^{-39} \text{ GeV}^{-1}$		$\text{Re}(c_{\mu\mu}^{(6)})$	$7 \times 10^{-45} \text{ GeV}^{-2}$	$(0:1:0)_S$
	$\text{Re}(a_{\mu\tau}^{(5)})$	$3 \times 10^{-38} \text{ GeV}^{-1}$		$\text{Re}(c_{\mu\tau}^{(6)})$	$1 \times 10^{-43} \text{ GeV}^{-2}$	$(0:1:0)_S$
	$\text{Re}(a_{\tau\tau}^{(5)})$	$2 \times 10^{-35} \text{ GeV}^{-1}$		$\text{Re}(c_{\tau\tau}^{(6)})$	$3 \times 10^{-36} \text{ GeV}^{-2}$	$(1/3:2/3:0)_S$
	$\text{Re}(a_{ee}^{(5)})$	$7 \times 10^{-40} \text{ GeV}^{-1}$		$\text{Re}(c_{ee}^{(6)})$	$2 \times 10^{-44} \text{ GeV}^{-2}$	$(1:0:0)_S$
	$\text{Re}(a_{e\mu}^{(5)})$	$4 \times 10^{-39} \text{ GeV}^{-1}$	$\text{Re}(c_{e\mu}^{(6)})$	$6 \times 10^{-45} \text{ GeV}^{-2}$	$(1:0:0)_S$	
	$\text{Re}(a_{e\tau}^{(5)})$	$2 \times 10^{-38} \text{ GeV}^{-1}$	$\text{Re}(c_{e\tau}^{(6)})$	$6 \times 10^{-45} \text{ GeV}^{-2}$	$(1:0:0)_S$	
7	$\text{Re}(a_{e\mu}^{(7)})$	$5 \times 10^{-46} \text{ GeV}^{-3}$	8	$\text{Re}(c_{e\mu}^{(8)})$	$1 \times 10^{-50} \text{ GeV}^{-4}$	$(0:1:0)_S$
	$\text{Re}(a_{e\tau}^{(7)})$	$4 \times 10^{-50} \text{ GeV}^{-3}$		$\text{Re}(c_{e\tau}^{(8)})$	$6 \times 10^{-56} \text{ GeV}^{-4}$	$(0:1:0)_S$
	$\text{Re}(a_{\mu\mu}^{(7)})$	$4 \times 10^{-50} \text{ GeV}^{-3}$		$\text{Re}(c_{\mu\mu}^{(8)})$	$5 \times 10^{-56} \text{ GeV}^{-4}$	$(0:1:0)_S$
	$\text{Re}(a_{\mu\tau}^{(7)})$	$2 \times 10^{-49} \text{ GeV}^{-3}$		$\text{Re}(c_{\mu\tau}^{(8)})$	$6 \times 10^{-55} \text{ GeV}^{-4}$	$(0:1:0)_S$
	$\text{Re}(a_{\tau\tau}^{(7)})$	$3 \times 10^{-45} \text{ GeV}^{-3}$		$\text{Re}(c_{\tau\tau}^{(8)})$	$3 \times 10^{-49} \text{ GeV}^{-4}$	$(1/3:2/3:0)_S$
	$\text{Re}(a_{ee}^{(7)})$	$8 \times 10^{-51} \text{ GeV}^{-3}$		$\text{Re}(c_{ee}^{(8)})$	$3 \times 10^{-55} \text{ GeV}^{-4}$	$(1:0:0)_S$
	$\text{Re}(a_{e\mu}^{(7)})$	$2 \times 10^{-49} \text{ GeV}^{-3}$	$\text{Re}(c_{e\mu}^{(8)})$	$5 \times 10^{-55} \text{ GeV}^{-4}$	$(1:0:0)_S$	
	$\text{Re}(a_{e\tau}^{(7)})$	$3 \times 10^{-49} \text{ GeV}^{-3}$	$\text{Re}(c_{e\tau}^{(8)})$	$8 \times 10^{-56} \text{ GeV}^{-4}$	$(1:0:0)_S$	

TABLE I. **Limits on new physics operators extracted from this analysis.** These limits on new physics operators are derived from Bayes factor > 31.6 which corresponds to 1 in 31.6 likelihood ratio for an equal prior. They are for characteristic source flavour ratios; $(1:0:0)_S$ and $(0:1:0)_S$. We list only operators where limits are set.

contributions to this manuscript from Carlos Argüelles, Kaareem Farrag, and Teppei Katori. The authors gratefully acknowledge the support from the following agencies and institutions: USA – U.S. National Science Foundation-Office of Polar Programs, U.S. National Science Foundation-Physics Division, U.S. National Science Foundation-EPSCoR, Wisconsin Alumni Research Foundation, Center for High Throughput Computing (CHTC) at the University of Wisconsin–Madison, Open Science Grid (OSG), Extreme Science and Engineering Discovery Environment (XSEDE), Frontera computing project at the Texas Advanced Computing Center, U.S. Department of Energy-National Energy Research Scientific Computing Center, Particle astrophysics research computing center at the University of Maryland, Institute for Cyber-Enabled Research at Michigan State University, and Astroparticle physics computational facility at Marquette University; Belgium – Funds for Scientific Research (FRS-FNRS and FWO), FWO Odysseus and Big Science programmes, and Belgian Federal Science Policy Office (Belspo); Germany – Bundesministerium für Bildung und Forschung (BMBF), Deutsche Forschungsgemeinschaft (DFG), Helmholtz Alliance for Astroparticle Physics (HAP), Initiative and Networking Fund of the Helmholtz Association, Deutsches Elektronen Synchrotron (DESY), and High Performance Computing cluster of the RWTH Aachen; Sweden – Swedish Research Council, Swedish Polar Research Secretariat, Swedish National Infrastructure for Computing (SNIC), and Knut and Alice Wallenberg Foundation; Australia – Australian Research Council; Canada – Natural Sciences and En-

gineering Research Council of Canada, Calcul Québec, Compute Ontario, Canada Foundation for Innovation, WestGrid, and Compute Canada; Denmark – Villum Fonden and Carlsberg Foundation; New Zealand – Marsden Fund; Japan – Japan Society for Promotion of Science (JSPS) and Institute for Global Prominent Research (IGPR) of Chiba University; Korea – National Research Foundation of Korea (NRF); Switzerland – Swiss National Science Foundation (SNSF); United Kingdom – Department of Physics, University of Oxford, the Royal Society, and the Science and Technology Facilities council (STFC).

* also at Università di Padova, I-35131 Padova, Italy

† also at National Research Nuclear University, Moscow Engineering Physics Institute (MEPhI), Moscow 115409, Russia

‡ also at Earthquake Research Institute, University of Tokyo, Bunkyo, Tokyo 113-0032, Japan

- [1] Y. Fukuda *et al.* (Super-Kamiokande), “Evidence for oscillation of atmospheric neutrinos,” *Phys. Rev. Lett.* **81**, 1562–1567 (1998), [arXiv:hep-ex/9807003 \[hep-ex\]](#).
- [2] Q. R. Ahmad *et al.* (SNO), “Measurement of the rate of $\nu_e + d \rightarrow p + p + e^-$ interactions produced by 8B solar neutrinos at the Sudbury Neutrino Observatory,” *Phys. Rev. Lett.* **87**, 071301 (2001), [arXiv:nucl-ex/0106015 \[nucl-ex\]](#).
- [3] M. G. Aartsen *et al.* (IceCube), “Evidence for High-Energy Extraterrestrial Neutrinos at the IceCube Detector,” *Science* **342**, 1242856 (2013), [arXiv:1311.5238 \[astro-ph.HE\]](#).
- [4] M. G. Aartsen *et al.* (IceCube), “Neutrino emission from the direction of the blazar TXS 0506+056 prior to the IceCube-170922A alert,” *Science* **361**, 147–151 (2018), [arXiv:1807.08794 \[astro-ph.HE\]](#).
- [5] S. W. Hawking, “The Unpredictability of Quantum Gravity,” *Commun. Math. Phys.* **87**, 395–415 (1982).
- [6] V. Alan Kostelecky and Stuart Samuel, “Spontaneous Breaking of Lorentz Symmetry in String Theory,” *Phys. Rev.* **D39**, 683 (1989).
- [7] G. Amelino-Camelia, John R. Ellis, N. E. Mavromatos, Dimitri V. Nanopoulos, and Subir Sarkar, “Tests of quantum gravity from observations of gamma-ray bursts,” *Nature* **393**, 763–765 (1998), [arXiv:astro-ph/9712103 \[astro-ph\]](#).
- [8] Maxim Pospelov and Yanwen Shang, “On Lorentz violation in Horava-Lifshitz type theories,” *Phys. Rev.* **D85**, 105001 (2012), [arXiv:1010.5249 \[hep-th\]](#).
- [9] M. G. Aartsen *et al.* (IceCube), “Neutrino Interferometry for High-Precision Tests of Lorentz Symmetry with IceCube,” *Nature Phys.* **14**, 961–966 (2018), [arXiv:1709.03434 \[hep-ex\]](#).
- [10] R. Abbasi *et al.* (IceCube), “The IceCube high-energy starting event sample: Description and flux characterization with 7.5 years of data,” (2020), [arXiv:2011.03545 \[astro-ph.HE\]](#).
- [11] R. Abbasi *et al.* (IceCube), “Measurement of Astrophysical Tau Neutrinos in IceCube’s High-Energy Starting Events,” (2020), [arXiv:2011.03561 \[hep-ex\]](#).
- [12] Jorge S. Diaz, Alan Kostelecky, and Matthew Mewes, “Testing Relativity with High-Energy Astrophysical Neutrinos,” *Phys. Rev.* **D89**, 043005 (2014), [arXiv:1308.6344 \[astro-ph.HE\]](#).
- [13] John Ellis, Nikolaos E. Mavromatos, Alexander S. Sakharov, and Edward K. Sarkisyan-Grinbaum, “Limits on Neutrino Lorentz Violation from Multimessenger Observations of TXS 0506+056,” *Phys. Lett.* **B789**, 352–355 (2019), [arXiv:1807.05155 \[astro-ph.HE\]](#).
- [14] V. Alan Kostelecky and Neil Russell, “Data Tables for Lorentz and CPT Violation,” *Rev. Mod. Phys.* **83**, 11–31 (2011), [arXiv:0801.0287 \[hep-ph\]](#).
- [15] Ivan Esteban, M. C. Gonzalez-Garcia, Michele Maltoni, Thomas Schwetz, and Albert Zhou, “The fate of hints: updated global analysis of three-flavor neutrino oscillations,” *JHEP* **09**, 178 (2020), [arXiv:2007.14792 \[hep-ph\]](#).
- [16] Alan Kostelecky and Matthew Mewes, “Neutrinos with Lorentz-violating operators of arbitrary dimension,” *Phys. Rev.* **D85**, 096005 (2012), [arXiv:1112.6395 \[hep-ph\]](#).
- [17] M. G. Aartsen *et al.* (IceCube), “The IceCube Neutrino Observatory: Instrumentation and Online Systems,” *JINST* **12**, P03012 (2017), [arXiv:1612.05093 \[astro-ph.IM\]](#).
- [18] Morihito Honda, T. Kajita, K. Kasahara, S. Midorikawa, and T. Sanuki, “Calculation of atmospheric neutrino flux using the interaction model calibrated with atmospheric muon data,” *Phys. Rev.* **D75**, 043006 (2007), [arXiv:astro-ph/0611418 \[astro-ph\]](#).
- [19] Atri Bhattacharya, Rikard Enberg, Mary Hall Reno, Ina Sarcevic, and Anna Stasto, “Perturbative charm production and the prompt atmospheric neutrino flux in light of RHIC and LHC,” *JHEP* **06**, 110 (2015), [arXiv:1502.01076 \[hep-ph\]](#).
- [20] D. Heck, J. Knapp, J. N. Capdevielle, G. Schatz, and T. Thouw, “CORSIKA: A Monte Carlo code to simulate extensive air showers,” (1998).
- [21] A. M. Dziewonski and D. L. Anderson, “Preliminary reference earth model,” *Phys. Earth Planet. Interiors* **25**, 297–356 (1981).
- [22] Amanda Cooper-Sarkar, Philipp Mertsch, and Subir Sarkar, “The high energy neutrino cross-section in the Standard Model and its uncertainty,” *JHEP* **08**, 042 (2011), [arXiv:1106.3723 \[hep-ph\]](#).
- [23] R. Abbasi *et al.* (IceCube), “LeptonInjector and LeptonWeighter: A neutrino event generator and weighter for neutrino observatories,” *Comput. Phys. Commun.* **266**, 108018 (2021), [arXiv:2012.10449 \[physics.comp-ph\]](#).
- [24] Ningqiang Song, Shirley Weishi Li, Carlos A. Argüelles, Mauricio Bustamante, and Aaron C. Vincent, “The Future of High-Energy Astrophysical Neutrino Flavor Measurements,” *JCAP* **04**, 054 (2021), [arXiv:2012.12893 \[hep-ph\]](#).
- [25] Rasmus W. Rasmussen, Lukas Lechner, Markus Ackermann, Marek Kowalski, and Walter Winter, “Astrophysical neutrinos flavored with Beyond the Standard Model physics,” *Phys. Rev.* **D96**, 083018 (2017), [arXiv:1707.07684 \[hep-ph\]](#).
- [26] Mauricio Bustamante and Sanjib Kumar Agarwalla, “Universe’s Worth of Electrons to Probe Long-Range Interactions of High-Energy Astrophysical Neutrinos,” *Phys. Rev. Lett.* **122**, 061103 (2019), [arXiv:1808.02042 \[astro-ph.HE\]](#).
- [27] Niki Klop and Shin’ichiro Ando, “Effects of a neutrino-dark energy coupling on oscillations of high-energy neutrinos,” *Phys. Rev.* **D97**, 063006 (2018), [arXiv:1712.05413 \[hep-ph\]](#).
- [28] Yasaman Farzan and Sergio Palomares-Ruiz, “Flavor of cosmic neutrinos preserved by ultralight dark matter,” *Phys. Rev.* **D99**, 051702 (2019), [arXiv:1810.00892 \[hep-ph\]](#).
- [29] Argüelles, Carlos A. and Katori, Teppei and Salvado, Jordi, “New Physics in Astrophysical Neutrino Flavor,” *Phys. Rev. Lett.* **115**, 161303 (2015), [arXiv:1506.02043 \[hep-ph\]](#).
- [30] F. Feroz, M. P. Hobson, and M. Bridges, “MultiNest: an efficient and robust Bayesian inference tool for cosmology and particle physics,” *Mon. Not. Roy. Astron. Soc.* **398**, 1601–1614 (2009), [arXiv:0809.3437 \[astro-ph\]](#).
- [31] Ruth Pordes, Don Petravick, Bill Kramer, Doug Olson, Miron Livny, Alain Roy, Paul Avery, Kent Blackburn, Torre Wenaus, Frank Würthwein, Ian Foster, Rob Gardner, Mike Wilde, Alan

Blatecky, John McGee, and Rob Quick, "The open science grid," in *J. Phys. Conf. Ser.*, 78, Vol. 78 (2007) p. 012057.

Supplementary Material

Appendix A: Analysis method

The notation of effective operators follows Ref. [9]. Explicitly, Eq. (1) can be written in following way,

$$H \sim \frac{m^2}{2E} + \begin{pmatrix} \overset{\circ}{a}_{ee}^{(3)} & \overset{\circ}{a}_{e\mu}^{(3)} & \overset{\circ}{a}_{\tau e}^{(3)} \\ \overset{\circ}{a}_{e\mu}^{(3)*} & \overset{\circ}{a}_{\mu\mu}^{(3)} & \overset{\circ}{a}_{\mu\tau}^{(3)} \\ \overset{\circ}{a}_{\tau e}^{(3)*} & \overset{\circ}{a}_{\mu\tau}^{(3)*} & \overset{\circ}{a}_{\tau\tau}^{(3)} \end{pmatrix} - E \cdot \begin{pmatrix} \overset{\circ}{c}_{ee}^{(4)} & \overset{\circ}{c}_{e\mu}^{(4)} & \overset{\circ}{c}_{\tau e}^{(4)} \\ \overset{\circ}{c}_{e\mu}^{(4)*} & \overset{\circ}{c}_{\mu\mu}^{(4)} & \overset{\circ}{c}_{\mu\tau}^{(4)} \\ \overset{\circ}{c}_{\tau e}^{(4)*} & \overset{\circ}{c}_{\mu\tau}^{(4)*} & \overset{\circ}{c}_{\tau\tau}^{(4)} \end{pmatrix} + \dots, \quad (\text{A1})$$

where, beyond the standard terms, there are two groups of new coefficients: the *CPT*-odd terms ($\overset{\circ}{a}^{(3)}$, $\overset{\circ}{a}^{(5)}$, $\overset{\circ}{a}^{(7)}$, ...) and the *CPT*-even terms ($\overset{\circ}{c}^{(4)}$, $\overset{\circ}{c}^{(6)}$, $\overset{\circ}{c}^{(8)}$, ...). The signs follow the convention of the Standard-Model Extension (SME) given in [16]. The integers in parentheses represent the dimension d of each operator. Hence, the units of these operators are GeV^{4-d} . The dimension-three and dimension-four operators are renormalizable, but all other operators are non-renormalizable. All effective operators affecting neutrino flavour conversions have Lorentz indices with time, spatial, and mixed components in the Sun-centred celestial equatorial frame (SCCEF) [14]. However, the astrophysical neutrino flux assumed in this analysis is the diffuse flux. Hence, we assume incoming neutrino directions are uniform. This averages out any spatial effects and so this analysis is only sensitive to the isotropic flux component. This is reflected in our notation by the circles on top of the operators indicating these operators are spatially isotropic.

In general, two or more operators with different dimensions (such as $\overset{\circ}{a}_{ee}^{(3)}$ and $\overset{\circ}{c}_{ee}^{(4)}$) may simultaneously affect the astrophysical neutrino flavour ratio. However, this is only relevant if the operator scales happen to have similar relative size in the energy region of this analysis; we hypothesise this as an unlikely coincidence and here we do not assume this possibility. To simplify this analysis, we take only one of the operators to be non-vanishing when reporting our results. It is also possible to assume two elements from the same dimensional operator (such as $\overset{\circ}{a}_{ee}^{(3)}$ and $\overset{\circ}{a}_{e\mu}^{(3)}$). Since all elements are complex numbers, limits can be set for both real and imaginary parts (such as $\text{Re}(\overset{\circ}{a}_{ee}^{(3)})$ and $\text{Im}(\overset{\circ}{a}_{ee}^{(3)})$). However, the available data statistics do not allow us to fit two operators with identical energy dimension simultaneously. Such assumptions were relaxed in Ref. [9]. There, it was found that the complex phase had a small effect on the limits. Hence, for this analysis we assume only search for one non-negative real element of each operator at a time.

The solution of the effective Hamiltonian (Eq. 1) is used to compute the flavour ratio. We follow the procedure outlined in Ref. [29]. First, neutrino flavour eigenstates $|\nu_\alpha\rangle$ can be described by the superposition of Hamiltonian eigenstates, $|\nu_i\rangle$,

$$|\nu_\alpha\rangle = \sum_i V_{\alpha i}(E) |\nu_i\rangle. \quad (\text{A2})$$

Here, $V_{\alpha i}(E)$ is a unitary transformation that diagonalizes the effective Hamiltonian (Eq. 1) to describe the mixing of neutrinos. Given the large baseline traversed and the energies involved, the resulting neutrino oscillation frequencies are very large and are averaged out by the detector energy resolution. In this regime, the transition probability of neutrinos can be written only through mixing matrix elements, which are the solution of the effective Hamiltonian. Explicitly, we find

$$P_{\nu_\alpha \rightarrow \nu_\beta}(E) = \sum_i |V_{\alpha i}(E)|^2 |V_{\beta i}(E)|^2. \quad (\text{A3})$$

The introduction of new interactions in vacuum through the new physics operators $\overset{\circ}{a}^{(3)}$, $\overset{\circ}{c}^{(4)}$, $\overset{\circ}{a}^{(5)}$, $\overset{\circ}{c}^{(6)}$, ... is imprinted in the mixing matrix element, $V_{\alpha i}(E)$, which can be determined through the neutrino mixing. The observable of interest is the neutrino flux of flavour β at Earth, $\phi_\beta^\oplus(E)$, and not the neutrino mixing itself. Note that the flux composition at Earth also depends on the initial neutrino flux of flavour α at the source, $\phi_\alpha^i(E)$. Furthermore, the small sample of astrophysical neutrinos restricts us to the use of the energy-averaged flavour composition,

$$\bar{\phi}_\beta^\oplus = \frac{1}{|\Delta E|} \int_{\Delta E} \sum_\alpha \bar{P}_{\nu_\alpha \rightarrow \nu_\beta}(E) \phi_\alpha^i(E) dE, \quad (\text{A4})$$

where we assume a single power-law spectrum for the production flux of astrophysical neutrinos and integrate it. Finally, we calculate the flavour ratio of astrophysical neutrino flavour β on Earth by normalizing it, *i.e.*,

$$f_\beta^\oplus = \bar{\phi}_\beta^\oplus / \sum_\gamma \bar{\phi}_\gamma^\oplus. \quad (\text{A5})$$

Appendix B: Systematic Errors and Fitting Method

In this analysis, a total of 14 systematic error nuisance parameters are simultaneously constrained. Firstly, the following six oscillation parameters [15]: two neutrino mass-square differences, $\Delta m_{21}^2 = 7.42_{-0.20}^{+0.21} (\times 10^{-5} \text{ eV}^2)$, $\Delta m_{31}^2 = 2.514_{-0.027}^{+0.028} (\times 10^{-3} \text{ eV}^2)$; three mixing angles, $\sin^2 \theta_{12} = 0.304_{-0.012}^{+0.013}$, $\sin^2 \theta_{23} = 0.570_{-0.024}^{+0.018}$, and $\sin^2 \theta_{31} = 0.02221_{-0.00062}^{+0.00068}$; and the Dirac CP -violating phase, δ_{CP} (no constraint). Second are five flux systematics which can be classified into two categories: the normalization of each flux component, and the spectral index assuming a single power law. The normalization systematic errors are introduced as shifts from the nominal predictions, including astrophysical neutrino flux (Φ_{astro} , no constraint), atmospheric neutrino conventional flux (Φ_{conv} , 40%), prompt flux (Φ_{prompt} , no constraint), and atmospheric muon flux (Φ_{muon} , 50%). The astrophysical neutrino spectral index (Φ_{astro} , no constraint) is also included as a systematic error, where this analysis returns a similar best fit value as in a dedicated study of the same sample [10]. We also introduce three detector systematic parameters: the DOM overall efficiency (ϵ_{DOM} , 10%), DOM angular dependence ($\epsilon_{\text{head-on}}$, 50%), and the in-ice photon propagation anisotropy around DOMs (a_s , 20%). Additional systematic errors arising from the modelling of atmospheric neutrinos and cosmic rays are used in other analyses [10, 11]. These systematics are not considered in this analysis because they mostly affect low-energy events ($<100 \text{ TeV}$). Here, the limit we set for QG-motivated physics depends on the highest end tail of the event distribution.

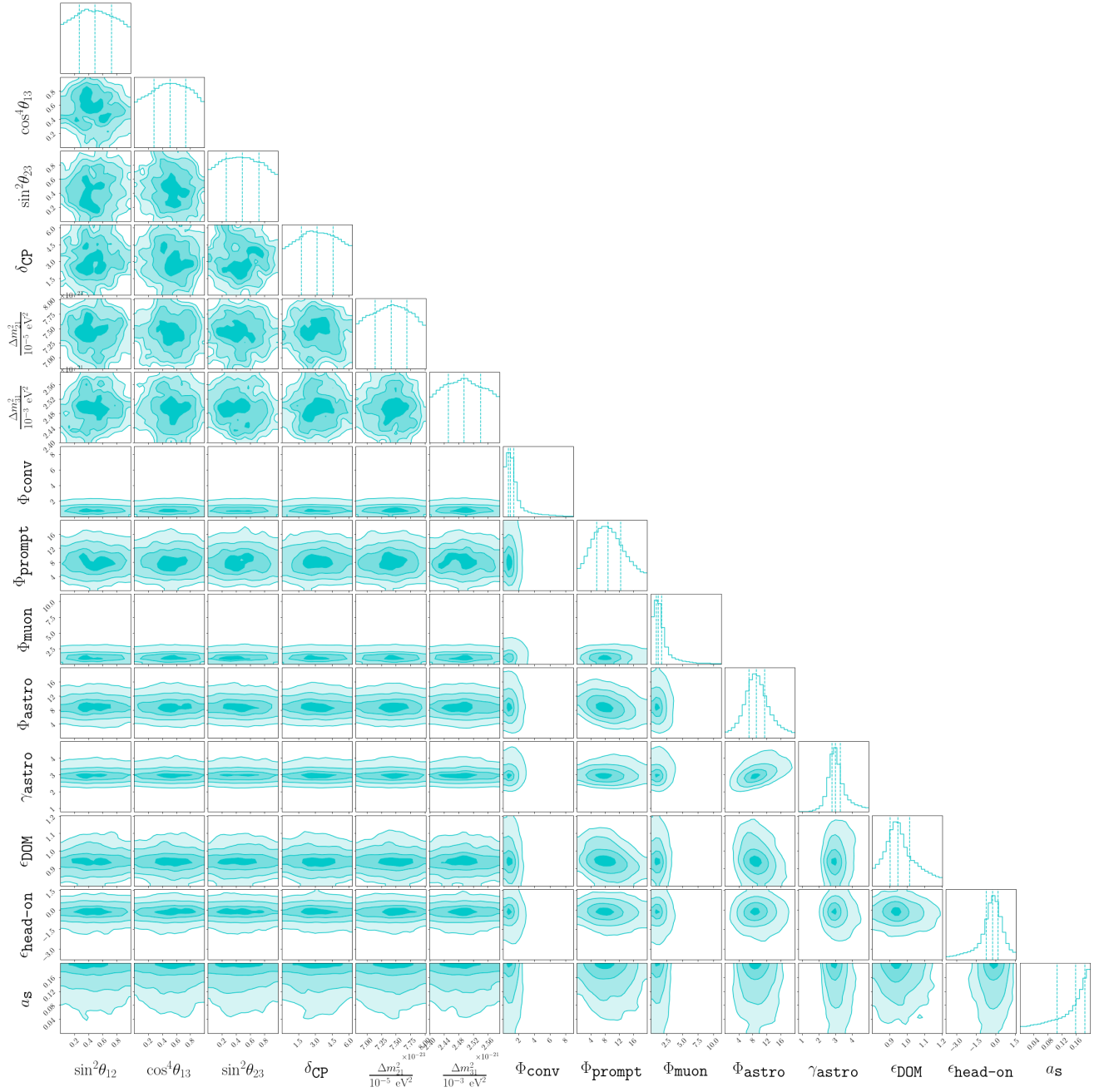
To place our limits we use two independent analysis methods based on frequentist and Bayesian approaches. The Bayesian approach was chosen to be the official result of this analysis due to its accuracy. The faster frequentist approach was used to check the Bayesian results. Both methods use the same 15-dimensional likelihood function with 14 systematic errors where one parameter represents a new physics scale. In the Bayesian case, the evidence is obtained by marginalising the same likelihood over the systematic parameters via a nested sampling. The marginalisation is done assuming model priors from [10]. We use the MultiNest algorithm [30] with 800 live points, approximately $\sim 18,000$ steps, and a tolerance of 0.05. Fig. 1 shows an example of a posterior distribution from one configuration. Here, the log-likelihood is calculated for $\text{Re}(\tilde{c}_{\tau\tau}^{(6)}) = 10^{-44} \text{ GeV}^{-2}$, with an assumed source flavour ratio $(1:0:0)_S$. We run nearly $\sim 200,000$ similar calculations with different configurations to map out the parameter phase space to find the signal.

We then define the Bayes factor to be the ratio of the model evidence with respect to the null hypothesis. We use Jeffreys' scale to set substantial and strong limits that are defined by the Bayes factor to be larger than 10.0 (substantial limit) and 31.6 (strong limit). Fig. 2 is an example of such a plot. Here, multiple sample runs are combined to construct a Bayes Factor distribution with a function of $\text{Re}(\tilde{c}_{\tau\tau}^{(6)})$ with an assumed source flavour ratio $(1:0:0)_S$. Due to limited statistics, simulated points have errors, and we use a spline function to extrapolate values between points. Table I list the strong limits from this procedure for selected source flavour ratio assumptions. Because of the extrapolation we used, we do not have enough accuracy to set limits and our results are presented with one digit.

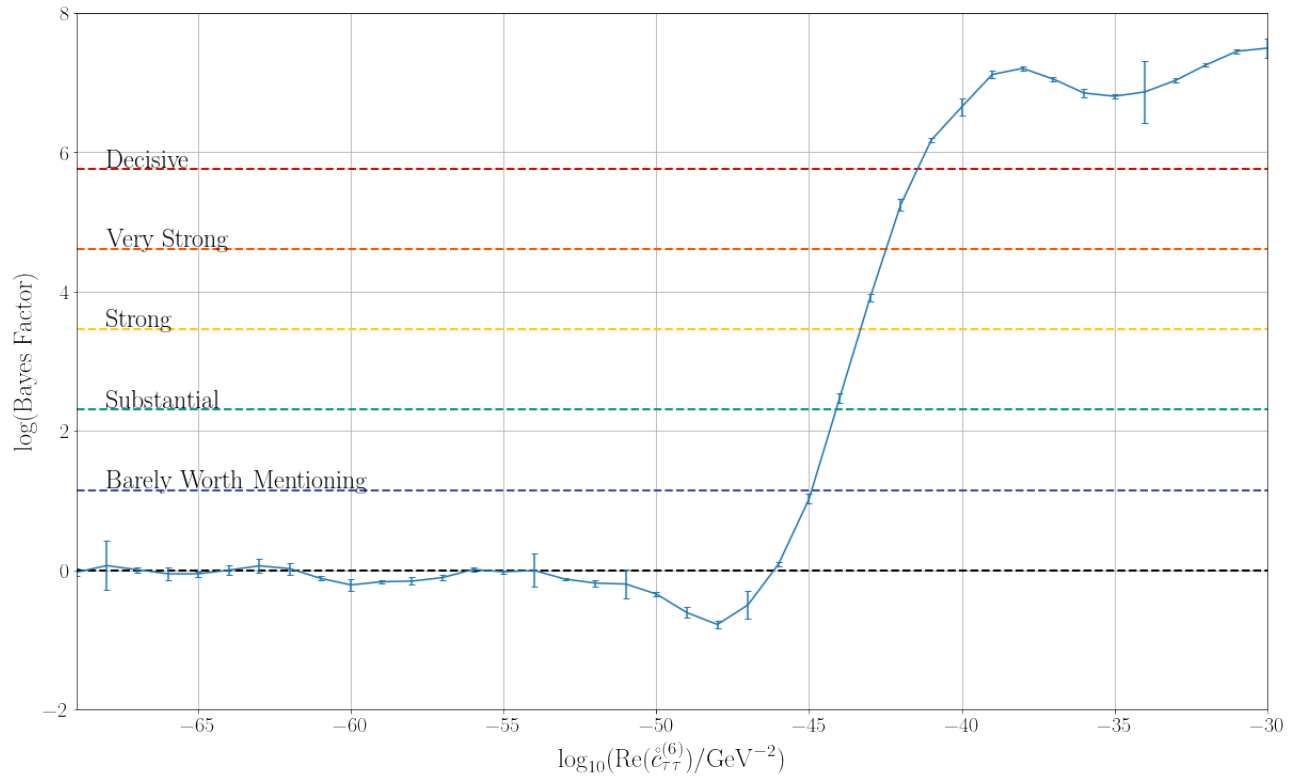
We repeat a similar Bayes Factor function construction with different source flavour ratio assumptions, and we construct the limits with a function of source flavour ratio x (Fig. 3). We use a spline function to extrapolate values between points and smooth the limit lines. We repeat this for different dimension operators, and these results are shown in Fig. 3. In the frequentist case, the likelihood function is used to find the best-fit point. Then, the profile likelihood ratio of the best fit to the null hypothesis is used to set limits assuming Wilks' theorem. However, Wilks' theorem may not hold in the full likelihood space which affect the limits obtained. We use distributed Open Science Grid [31] computational resources to perform both analyses.

Appendix C: Results With Other New Physics Operators

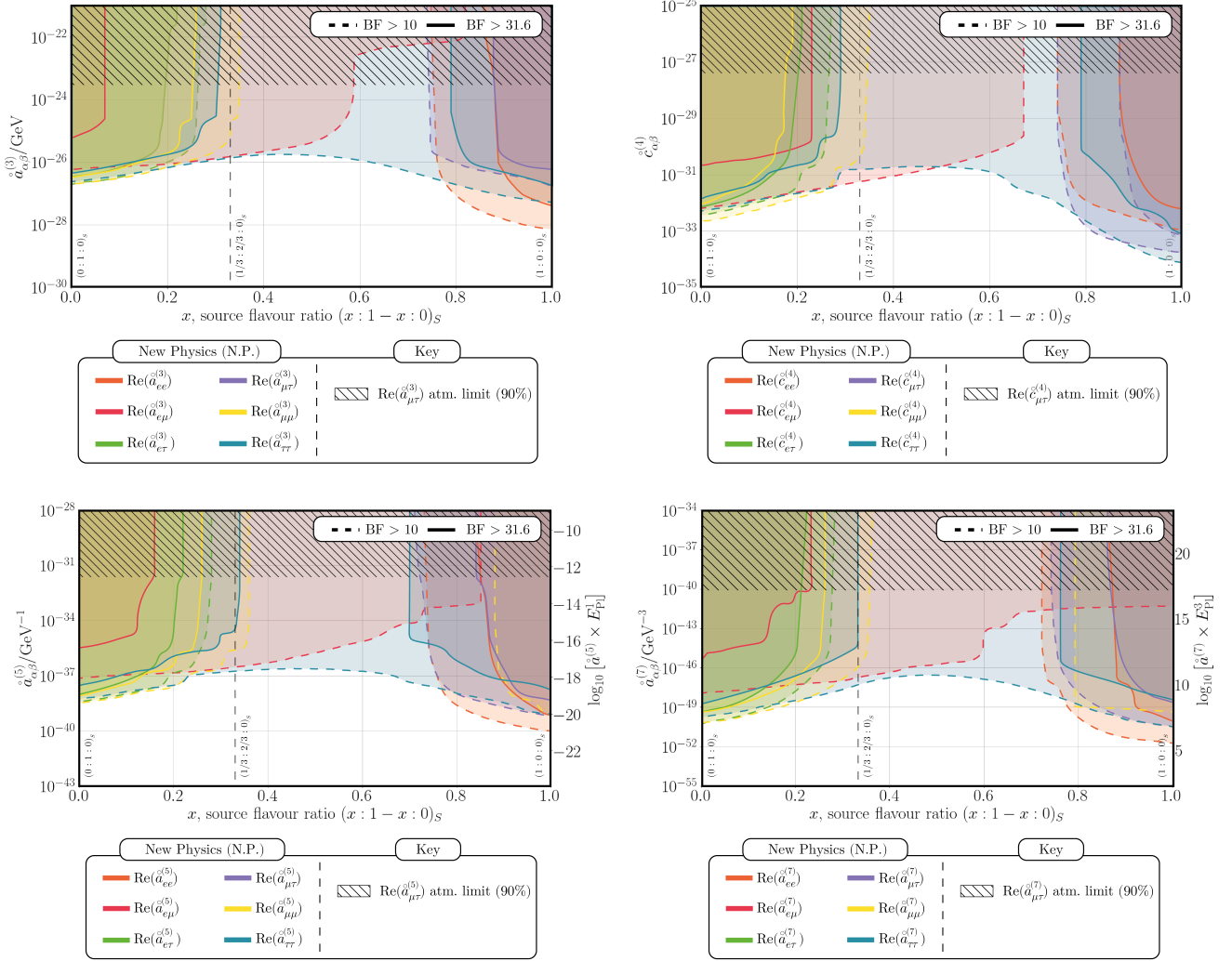
Fig. 3 summarises the results for each dimension coefficient studied. Although this analysis provides the most stringent limits for a wide range of assumed source compositions, an analysis using atmospheric neutrinos [9] can provide limits for a certain region. The limits of this analysis go stronger for higher dimensions due to the stronger energy dependence (Eq. (1)). As the dimension increases, limits from astrophysical neutrino interferometry become significantly stronger than atmospheric neutrino interferometry. On the other hand, for dimension seven and higher operators, QG-motivated physics is expected to be smaller than E_p^{-3} and E_p^{-4} . This analysis has no sensitivity to the operators with these sizes. The dimension-three and -four operators are renormalizable and we cannot define QG-motivated physics in the same way.



SUPPL. FIG. 1. Example posterior distribution over the 14 nuisance parameters for $\text{Re}(\hat{c}_{\tau\tau}^{(6)}) = 10^{-44} \text{ GeV}^{-2}$ with source combination $(1:0:0)_S$. Here, blue contours show two dimensional distribution slices, with one-dimensional projections above for each parameter. Three vertical lines indicate the lower quartile (25%), median (50%) and upper quartile (75%) for each parameter.



SUPPL. FIG. 2. Example of the analysis Bayes factor as a function of one of the constrained parameters. Horizontal lines show different hypothesis rejection strength levels according to Jeffrey’s scale. Here, we set the limit on $\text{Re}(c_{\tau\tau}^{(6)})$ with an assume source flavour ratio $(1 : 0 : 0)_S$. Substantial limit is obtained when the Bayes Factor is greater than 10.0, and strong limits when the Bayes Factor is greater than 31.6. Error bars indicate the error on the evidence computation via nested sampling.



SUPPL. FIG. 3. **Limits on the dimension-three, -four, -five, and -seven new physics operators.** The hatched region is the limit obtained from the atmospheric neutrino data analysis on $\text{Re}(\hat{a}_{\mu\tau}^{(d)})$ [9]. Limits are presented as a function of the assumed astrophysical neutrino flavour ratio at the production source. The leftmost scenario is ν_μ dominant $(0:1:0)_S$ and the rightmost is ν_e dominant $(1:0:0)_S$. The preferred scenario corresponds to $(1/3:2/3:0)_S$ (dashed vertical line). Limits on $\text{Re}(\hat{a}_{ee}^{(d)})$ (orange), $\text{Re}(\hat{a}_{e\mu}^{(d)})$ (red), $\text{Re}(\hat{a}_{e\tau}^{(d)})$ (green), $\text{Re}(\hat{a}_{\mu\mu}^{(d)})$ (yellow), $\text{Re}(\hat{a}_{\mu\tau}^{(d)})$ (purple), and $\text{Re}(\hat{a}_{\tau\tau}^{(d)})$ (blue) are shown when $d = 3, 4, 5$ or 7 .